Lead-free nanocomposite piezoelectric nanogenerator film for biomechanical energy harvesting

Zouhair Hanani, Ilyasse Izanzar, M'Barek Amjoud, Daoud Mezzane, Mohammed Lahcini, Hana Uršič, Uroš Prah, Ismaël Saadoune, Mimoun El Marssi, Igor A. Luk'Yanchuk, et al.

Lead-free Nanocomposite Piezoelectric Nanogenerator Film for Biomechanical Energy Harvesting

Zouhair Hanani,[a,b] Ilyasse Izanzar,[a] M'barek Amjoud,[a] Daoud Mezzane,[a] Mohammed Lahcini,[a,c] Hana Uršič,[d] Uroš Prah,[d] Ismael Saadoune,[a] Mimoun El Marssi,[e] Igor A. Luk'yanchuk,[e,f,*] Zdravko Kutnjak,[d] and Mohamed Gouné[b]

[a] IMED-Lab, Cadi Ayyad University, Av. A. El Khattabi, P.B. 549, Marrakesh, 40000, Morocco

[b] ICMCB, University of Bordeaux, 87 Avenue du Dr Albert Schweitzer, Pessac, 33600, France

[c] Mohammed VI Polytechnic University, Lot 660-Hay Moulay Rachid, Ben Guerir, 43150, Morocco

[d] Jožef Stefan Institute, Jamova cesta 39, Ljubljana, 1000, Slovenia

[e] LPMC, 33 rue Saint Leu, University of Picardy Jules Verne, Amiens, 80039, France

[f] Department of Building Materials, Kyiv National University of Construction and Architecture, Kyiv, Ukraine

[*] corresponding author : lukyanc@ferroix.net

Abstract

Piezoelectric nanogenerators are attracting substantial attention due to the environmental constraints and ecological considerations of energy harvesting. However, the Achilles' heel of the majority of these nanogenerators is the presence of toxic compounds or the requirement of a poling process to promote higher piezoelectric effect. Here a self-poled and bio-flexible piezoelectric nanogenerator (BF-PNG) is designed, based on lead-free biocompatible $Ba_{0.85}Ca_{0.15}Zr_{0.10}Ti_{0.90}O_3$ nanoparticles functionalized with polydopamine embedded in the polylactic acid biodegradable polymer. The BF-PNG can generate open-circuit voltage and short-circuit current of 14.4 V and 0.55 µA, respectively, under gentle finger tapping. Furthermore, it demonstrates an outstanding high mechanical robustness and stable output voltage after 14000 cycles. It achieves a maximum power density of about 7.54 mW/cm^3 at a low resistive load of 3.5 MΩ. The feasibility of the BF-PNG by trigging commercial electronics such as charging capacitors and lighting a LED is verified, and the BF-PNG can drive a 1 µF capacitor to store the energy of 3.92 µJ within 115 s under gentle finger tapping. This research demonstrates that a lead-free piezoceramic in combination with a biodegradable piezopolymer can lead to a design of bio-flexible piezoelectric nanogenerators with outstanding performances and in particular useful in self-powered medical devices.

Keywords: self-poled piezoelectric nanogenerator, core/shell nanoparticles, polylactic acid, biocompatible, nanocomposite

1. Introduction

Because of their robustness and their enhanced output performances, the ceramic/polymer nanocomposite piezoelectric nanogenerators (PNGs) using piezoelectric materials at the nanoscale are in the focus of development of the new generation of mechanical energy-harvesting sources [1–4]. Importantly, these PNGs could drive self-powered and wireless healthcare systems such as heart monitor, pacemaker energizer, blood flow monitor, and real-time biomedical monitor [5–9]. Today's market of piezoelectric devices is dominated mainly by lead-based piezoceramics like $PbZr_xTi_{1-x}O_3$ (PZT) and (1- x)$Pb(Mg_{1/3}Nb_{2/3})O_3$−$xPbTiO_3$ (PMN−PT) systems because of their excellent piezoelectric properties [5,10,11]. However, the toxicity of lead and harmfulness to the environment and human health [12–14] makes the replacement of PZT by the homologs with comparable piezoelectric properties but without lead as an urgent task [15–18]. In this regard, lead-free bioceramic $Ba_{0.85}Ca_{0.15}Zr_{0.10}Ti_{0.90}O_3$ (BCZT), is considered as a potential candidate to substitute the lead-based materials [13,19–22]. Notably, this material was shown to demonstrate the enhanced dielectric, ferroelectric and piezoelectric performances [22–26]. Another important factor of BCZT ceramics is biocompatibility nature [27–29]. Scarisoreanu et al. [29] proved for the first time that BCZT coatings on Kapton polymer substrates could provide optimal support for osteogenic differentiation of mesenchymal stem cells in the bone marrow.

The particular interest presents the embedding of the BCZT materials into the matrix of Polylactic acid (PLA) which is a low cost, biodegradable, and biocompatible polymer with excellent mechanical properties, chemical, and electrical resistance, and it is amenable to a variety of processing techniques [30,31]. PLA is a polymer known for many years in the field of medical applications such as sutures, orthopedic pins, or galenics [32]. PLA is now available for mass markets such as for packaging, single-use items, fibers, etc. New developments in terms of products are underway and should soon enable PLA to be more present in sustainable applications such as the automotive sector, floor coverings, electronics, etc. [33,34]. PLA is becoming a promising candidate for energy harvesting applications owing to its high piezoelectric properties, which could outspread the applications of PNGs to several energy-related systems, namely in the biomedical field [35–37]. The carbonyl groups present in PLA structure induce polarity, and it shows a piezoelectric coefficient d_{14} value of 10 pC/N without an additional poling step in its crystalline structure [38]. Curry et al. [39] elaborated a biodegradable and flexible piezoelectric force sensor based on poly-l-lactide (PLLA) polymer for measurement of physiological pressures such as lung pressure, brain pressure and eye pressure. Zheng et al. [40]

reported the concept of a biodegradable triboelectric nanogenerator (BD-TENG) for short-term *in vivo* biomechanical energy conversion based on available low-cost polymers.

BCZT ceramics were elaborated extensively by solid-state reaction and sol-gel processing at high temperatures due to its simplicity, we have demonstrated that the synthesis temperature of BCZT powders could be decreased to a low temperature of 160 °C while still preserving enhanced dielectric, ferroelectric and energy storage properties [41,42]. This temperature is about 1200 °C lower when compared with solid-state reaction and is about 840 °C lower than in sol-gel methods, which is a valuable asset in large-scale industrial production [41].

In the current article, a flexible piezoelectric nanogenerator (BF-PNG) combining BCZT nanopowders functionalized with polydopamine (PDA) via core-shell structuration (BCZT@PDA) and PLA biopolymer, was designed without any poling process. The outputs performances under different human body motions were tested, alongside with the feasibility of the BF-PNG to drive commercial electronics (charging capacitors and glowing a light-emitting diode (LED)). The fabricated BF-PNG could generate open-circuit voltage and short-circuit current of 14.4 V and 0.55 µA, respectively, under gentle finger tapping, and demonstrated an outstanding high mechanical robustness and stable output voltage after 14000 cycles of high-frequency impartations.

2. Experimental Section

2.1. Preparation of BCZT@PDA/PLA nanocomposite film

$Ba_{0.85}Ca_{0.15}Zr_{0.10}Ti_{0.90}O_3$ (BCZT) nanocrystalline and the pure powder was obtained through a sol-gel method followed by a single-step hydrothermal synthesis in a high alkaline medium at 160 °C for 24 has reported previously [43]. Additional characterization data of BCZT ceramic like structural, dielectric, and ferroelectric properties can be found in Refs [41,43]. A layer of polydopamine (PDA) was coated on BCZT nanoparticles to form functionalized BCZT@PDA nanoparticles with enhanced dispersion stability, i.e., to avoid the agglomeration. Detailed experimental procedure and morphology of BCZT@PDA nanoparticles before and after the core-shell structuration are presented in the S2 section and Fig. S1 in the Supporting Information, respectively. BCZT@PDA/PLA nanocomposite film was elaborated by the solution casting method using 20 vol% of BCZT@PDA nanoparticles dispersed in the PLA matrix. The detailed experimental procedure for the preparation of BCZT@PDA/PLA nanocomposite film is depicted in the S3 section (Supporting Information).

2.2. Fabrication of the BF-PNG

The BCZT@PDA/PLA nanocomposite film was sandwiched between two copper foils of 1.5 × 1.3 cm^2 serving as top and bottom electrodes. For external connections, two copper wires were attached to the top and bottom electrodes to measure the open-circuit voltage and short-circuit current. Then, the BF-PNG was additionally sandwiched by using the Kapton tape. This encapsulation prevented damage of the BF-PNG by repeated mechanical excitations and made it water- and dustproof.

2.3. Instrumentations and Setups

Transmission electron microscope (JEOL - ARM 200F Cold FEG TEM/STEM) operating at 200 kV coupled with a high-angle annular dark-field (HAADF) detector was used to visualize the thickness of PDA coating on the surface of BCZT nanoparticles. The local piezoelectric responses of BCZT@PDA nanoparticles before and after embedding in the PLA matrix were investigated with an atomic force microscope (AFM, Asylum Research, MFP-3D) equipped with a piezo-response force module (PFM). To avoid the sticking of the BCZT@PDA nanoparticles to the PFM tip, the particles were fixed using epoxy resin as previously reported in ref [44]. A Ti/Ir-coated Si tip with a radius of curvature ~20 nm (Asyelec, Atomic Force F&E GmbH) was utilized, and the electric field was applied to the sample in the virtual ground regime, similarly as previously reported in refs [44,45]. The out-of-plane piezo-response amplitude images of BCZT@PDA nanoparticles before and after embedding in the PLA matrix were recorded in dual ac-resonance tracking mode at an ac amplitude signal of 60 V and ~350 kHz. The PFM amplitude and phase hysteresis loops were measured in the switching spectroscopy off-electric field mode with the pulse dc step signal and overlapped drive ac signal. The waveform parameters were as follows: the sequence of increasing dc electric field steps was driven at 20 Hz with a maximum amplitude of 150–200 V; the frequency of the triangle envelope was 200 mHz; an overlapping ac sinusoidal signal with an amplitude of 5 or 10 V and a frequency of ~350 kHz was used. Three cycles were measured in an off-electric field mode. The average thickness of the nanocomposite film was measured by a precise coating thickness gauge (Surfix Pro S, Phynix), and proved by using a field-emission scanning electron microscope (FESEM, JEOL 7600F). To study the output performances of the BCZT@PDA/PLA piezoelectric nanogenerator, the open-circuit voltage (V_{oc}) and the short-circuit current (I_{sc}) were measured by using a multi-channel, research grade battery cycler (MPG-2, Bio-Logic). The approximate contact forces of finger tapping and hand slapping were evaluated experimentally by using a dual column mechanical testing system (Instron, 3369). All measurements were carried out at room temperature.

3. Results and Discussions

3.1. Local piezoelectric properties

The piezoelectric response which is the key property of PNGs, was carefully checked before and after embedding BCZT@PDA nanoparticles in the PLA matrix by piezoresponse force microscopy (PFM). The PFM is based on the detection of a local electromechanical response of the ferroelectric material through the converse piezoelectric effect. Fig. 1 shows the schematics of the PFM setup and BCZT@PDA/PLA nanocomposite film.

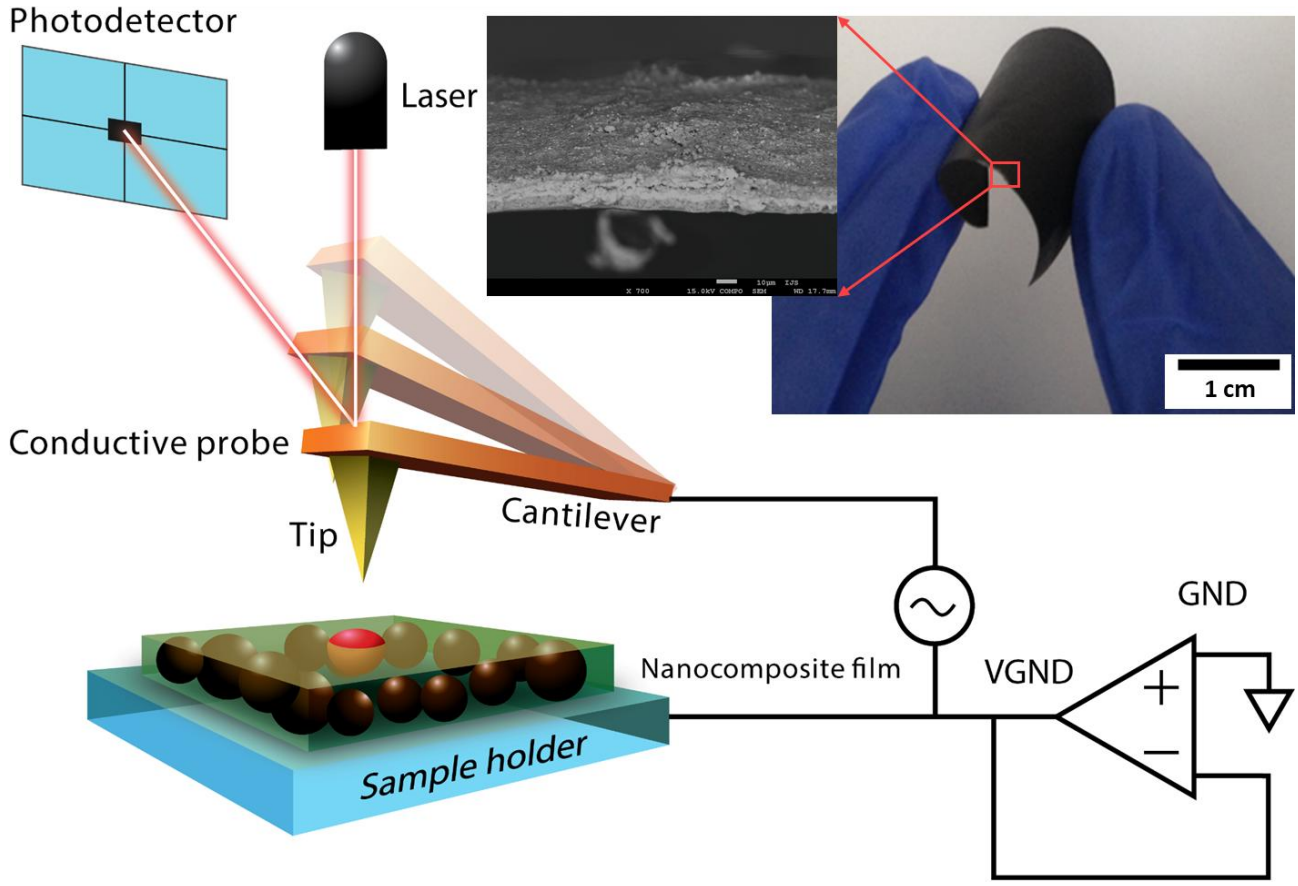

Fig. 1. The operating setup used to measure the piezoelectric response in BCZT@PDA/PLA nanocomposite film schematically shown in the upper right corner (zoomed inset displays field-emission scanning electron microscope (FESEM) image of the nanocomposite film).

Before the incorporation of BCZT@PDA nanofillers in the PLA matrix, the topographic AFM and the out- of- plane amplitude PFM images are shown in Figs. 2a-h. The single particles can be clearly distinguished in topography (a) height and (b) deflection images. PFM amplitude and phase images show that the BCZT@PDA particles are piezoelectrically active. A closer look (Figs. 2e-h) reveals inside the particle's regions of different piezoelectric activity (white arrows mark some examples). To further investigate piezoelectric/ferroelectric responses, PFM switching spectroscopy experiment was

performed. The local phase and amplitude hysteresis loops typical for piezoelectric/ferroelectric material were measured, as shown in Figs. 2i, j.

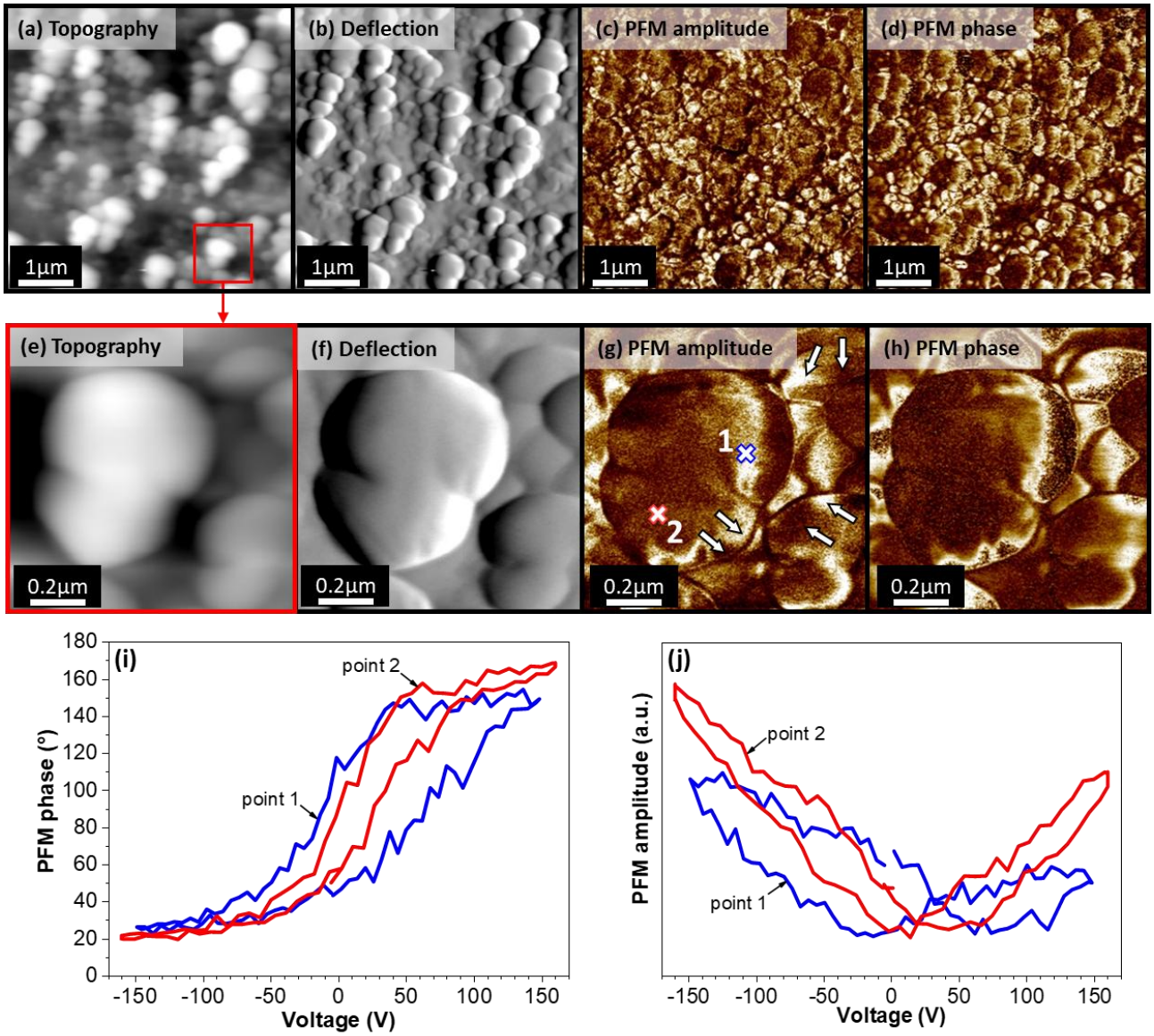

Fig. 2. The topography (a, e) height, (b, f) deflection and out-of-plane PFM (c, g) amplitude, (d, h) phase images of BCZT@PDA nanoparticles. The PFM (i) phase and (j) amplitude local hysteresis loops measured in the two points 1 and 2 marked by crosses in panel (g). In both panels (i and j), a second cycle is shown.

The local piezoelectric response and local domain switching properties of BCZT@PDA powder inserted in the PLA polymer matrix forming 20 vol% BCZT@PDA/PLA nanocomposite film were investigated by using the PFM (see Fig. 3a-g). The topography, out-of-plane amplitude, and phase signals were analyzed (see Fig. 3a-d). By comparing the topography and amplitude PFM images, we

can conclude that the enhancements in the PFM signal (bright regions) are observed at the positions of the BCZT@PDA powder islands, indicating their piezoelectric activity. Additionally, the PFM switching spectroscopy experiment was performed on the BCZT@PDA powder island in two points (see Fig. 3e). The local PFM phase and amplitude hysteresis loops typical for piezoelectric/ferroelectric material are shown in Fig. 3f and 3g. Hence, the local piezoelectric response of 20 vol% BCZT@PDA/PLA nanocomposite film was confirmed.

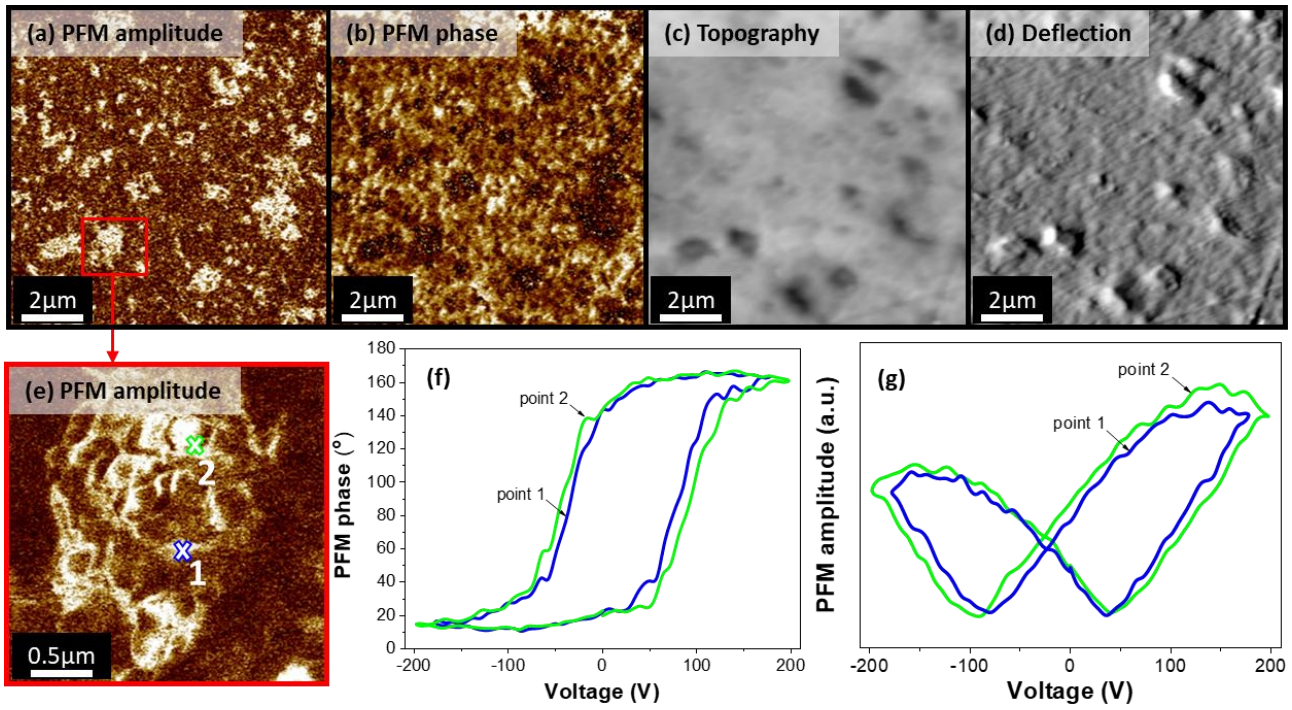

Fig. 3. Out-of-plane PFM (a) amplitude, (b) phase images with the topography (c) height and (d) deflection of 20 vol% BCZT@PDA/PLA film. In the panel (a), the bright regions are the BCZT@PDA powder islands embedded in the darker PLA matrix. The large magnification of such an island is shown in panel (e). The panels (f) and (g) show phase and amplitude of local hysteresis loops, respectively, measured by PFM in the two points, marked by crosses 1 and 2 in the panel (e). In both panels (f and g), a second cycle is shown.

3.2. Mechanical energy harvesting

Generally, PNGs are used to harvest mechanical energy in a relatively low-frequency range (e.g., human activities, mechanical vibration, etc.). Here, the stress field (σ) plays a vital role in the generation of output voltage as the deformation of the crystal structure depends on applied mechanical stress. In this study, two types of human impartations were investigated: the finger tapping and hand slapping under fixed frequency. The approximate contact force was evaluated experimentally by using

a dual column mechanical testing system. The average contact forces (F) were estimated at 2.0 N and 27.9 N for the finger tapping and hand slapping, respectively, and the results are shown in Figs. 4a, b. The resulting input stress (σ) under finger tapping and hand slapping is estimated using $\sigma = F/area$, and found to be 9.1 kPa (contact area ~2.2 cm^2) and 18.5 kPa (contact area ~15.1 cm^2), respectively. A demonstration for the contact force measurement under finger tapping is depicted in Video S1 (Supporting Information).

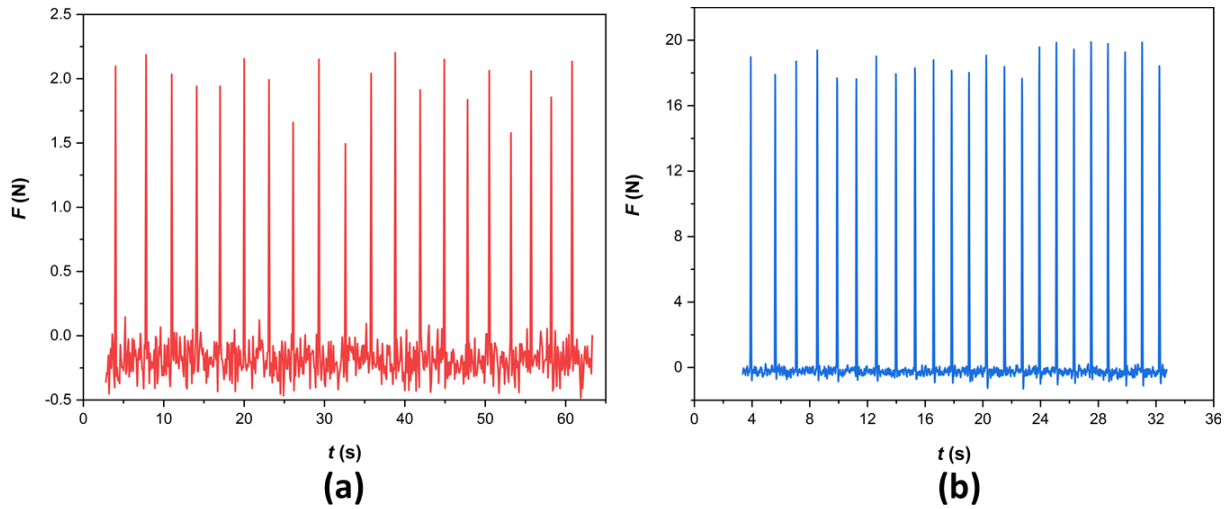

Fig. 4. The measured contact force under (a) finger tapping and (b) hand slapping.

To have an insight into the mechanical energy harvesting performances of BCZT@PDA/PLA piezocomposite film from the energy available in the ambient environment (human body motions), a bio-flexible piezoelectric nanogenerator (BF-PNG) was designed. The schematic illustration and the photo of the flexible BF-PNG generator device are shown in Figs. 5a, b, respectively. The fabrication process of the BF-PNG is described in the Experimental Section. Besides, the open-circuit voltage (V_{oc}) and the short-circuit current (I_{sc}) for the BF-PNG were measured. Figs. 5c, d show the V_{oc} and the I_{sc}, respectively, of the BF-PNG subjected to a series of gentle finger tapping as demonstrated in the Video S2 in the Supporting Information. By finger tapping, the V_{oc} and I_{sc} of the BF-PNG can reach values up to 14.40 V and 0.55 µA, respectively. The slight variation in the amplitude of each pulse could be attributed to the manual stress variation during the tapping sequence. It should be noted that these values are comparable to those found in PNGs containing other types of piezoelectric materials [46–49]. The working mechanism of the BF-PNG is discussed in section S4 (Supporting Information). It should be noted that contrary to polyvinylidene fluoride (PVDF) or polydimethylsiloxane (PDMS) based PNGs, no poling process is required before testing the PNG as the BF-PNG is a self- poled device. It benefits from the natural piezoelectricity developed in PLA after application of mechanical

stress and the surface-charge induced polarization without applying any external electric field [35,50,51]. Hence, in BF-PNG, the traditional electrical poling process used in piezoelectric and ferroelectric materials-based energy harvesting devices is not required.

The voltage-stability test of the fabricated BF-PNG was performed under gentle finger tapping at a driving frequency of 0.3 Hz for 115 s (Fig. 5e), and under 14000 tapping cycles by using a sewing machine at tapping frequency of 23 Hz for 625 s (Fig. 5f). See also demonstrations in Videos S2 and S3 in the Supporting Information. The sewing machine was used as a constant stress source compared to finger tapping and hand slapping. Here, the sewing machine needle was substituted by a cylindrical plastic piece with a tapping area close to that of a human finger. In this case, the BF-PNG was exposed to direct stress tapping indicating its high mechanical stability. It is worth noting that neither performance degradation nor mechanical damage after 14000 cycles at a frequency of 23 Hz was observed. The mechanical robustness and the excellent stability of the BF-PNG signal without a significant drop in V_{oc} prove its applicability as a capable energy harvesting device of irregular and regular excitations present in our living environment and as a powering device for small portable electronic applications and flexible high energy density capacitors. Various tests were devoted to verify the potential use of the BF-PNG for operating commercial electronic devices.

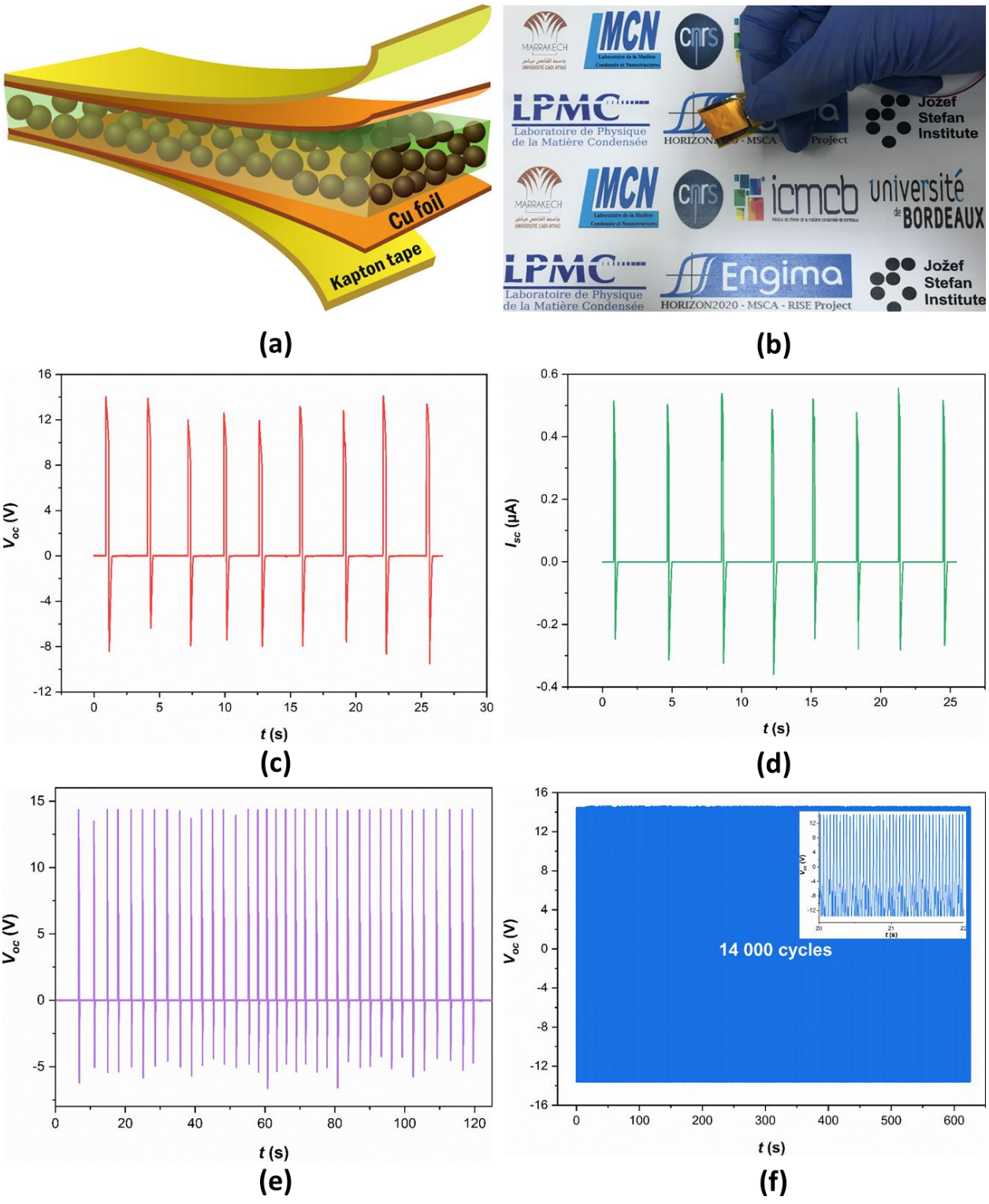

Fig. 5. (a) Schematic illustration of the prepared composite generator and (b) a photograph of the flexible nanocomposite generator device (BF-PNG). The generated (c) open-circuit voltage and (d) short-circuit current of the BF-PNG under finger tapping, and the results of voltage stability tests of the BF-PNG device under (e) finger tapping and (f) under 14000 tapping cycles using a sewing machine (inset shows a magnified view of the voltage stability).

3.3 Charge-storage capability of BF-PNG

The power and accumulation tests checked the feasibility of the BF-PNG device for the application. To evaluate the energy storage capability of the BF-PNG device, one cycle of charging and discharging was performed on a commercial capacitor (1 μF) under finger tapping and hand slapping with a frequency of 4 Hz as shown in Fig. 6a. The inset of Fig. 6b illustrates the schematic circuit diagram for the following of the accumulated voltage during capacitor charging, which includes a full-wave bridge rectifier, capacitor, and BF-PNG. The ac output generated by the BF-PNG was first converted into dc power through the rectifier, then the generated dc power was used to charge the capacitor. The enlarged plot of accumulated voltage-time charging curves under (inset of Fig. 6a) shows stepwise charging of the capacitor under both human body motions. In the case of finger tapping and hand slapping, the BF-PNG could charge the capacitor up to 2.27 and 4.94 V, respectively, which correspond according to $U_e = 1/2\,CV^2$, to stored energy of 2.57 and 12.20 μJ, respectively (Fig. 6b). Here U_e, C, and V correspond to the stored electric density, capacitor capacity, and the generated voltage, respectively. The equivalent energy density using finger tapping and hand slapping reached 0.775 and 3.68 mJ/cm^3, respectively. This latter is 1.7 times higher than that found by Shin et al. [52] in BZT–BCT NPs/PVDF composite film.

To characterize the output performance of PNGs, the output charge density is an important parameter, though, most works about PNG do not report the output charge density. The corresponding average charging rate is 7.7 and 42.2 nC per cycle, equivalent to 39.5 and 215.8 μC/m^2, for finger tapping and hand slapping, respectively. The output charge density and the generated energy in the case of hand slapping are more significant due to the higher input stress (σ =18.5 kPa). The obtained value of the output charge density in the case of hand slapping is higher than that found by Gu et al. [53] (193 μC/m^2) in PNG with a three-dimensional intercalation electrode (IENG) using foot stepping. Moreover, our BF-PNG demonstrated higher output charge density compared to some reported triboelectric nanogenerators (TENGs) [54–56]. The real-time recording of the accumulated voltage across the capacitor under finger tapping and hand slapping is presented in Videos S4 and S5 in the Supporting Information, respectively. It is worthy to note that the unsmooth charging curves, especially, during hand slapping is originated from the inhomogeneous motions. To overcome this drawback, the sewing machine was used as a nearly constant stress source compared to a human finger. The charging capability of the BF-PNG under constant stress source was tested by storing a rectified electrical output from the BF-PNG in two commercial capacitors of 1 μF and 2.2 μF. Three charge-discharge cycles were performed to prove the performance reproducibility of the BF-PNG. The charging and

discharging behavior of the capacitors 1 µF (Fig. 6c) and 2.2 µF (Fig. 6d) at a constant frequency of 23 Hz. The insets of Fig. 6c and d display the enlarged views of the charging behavior of the capacitor. The typical stepwise charging and the discharging response of the capacitor signify the high energy storage capacity. The BF-PNG could charge the 1 µF-capacitor up to 6.36 V within 18.4 s only, which corresponds to stored energy of 20.22 µJ. The discharging process requires more time than charging one. Hence, three discharging cycles were performed for discharging down to 3 V. This implies that the fabricated BF-PNG device could be used to recharge discharged batteries. Furthermore, it can also be seen that the fabricated device can charge the capacitor several times, which proves the reproducibility of the BF-PNG under cyclic charging and discharging conditions. The charging and discharging behavior of a commercial capacitor of 2.2 µF are shown in Fig. 6d. After 52 s of impartation, the 2.2 µF capacitor reached a voltage of 3.38 V, which corresponds to the stored energy of 12.56 µJ. The charging and discharging experiment were carried three times wherein each step the maximum voltage of the capacitor reached up to 3.52 V, which also proves the reproducibility of the BF-PNG. From these results, we can conclude that the capacitors of different capacitance can be charged up by the BF-PNG to a certain voltage under specific time and with high stored energy, which will be useful for further utilization.

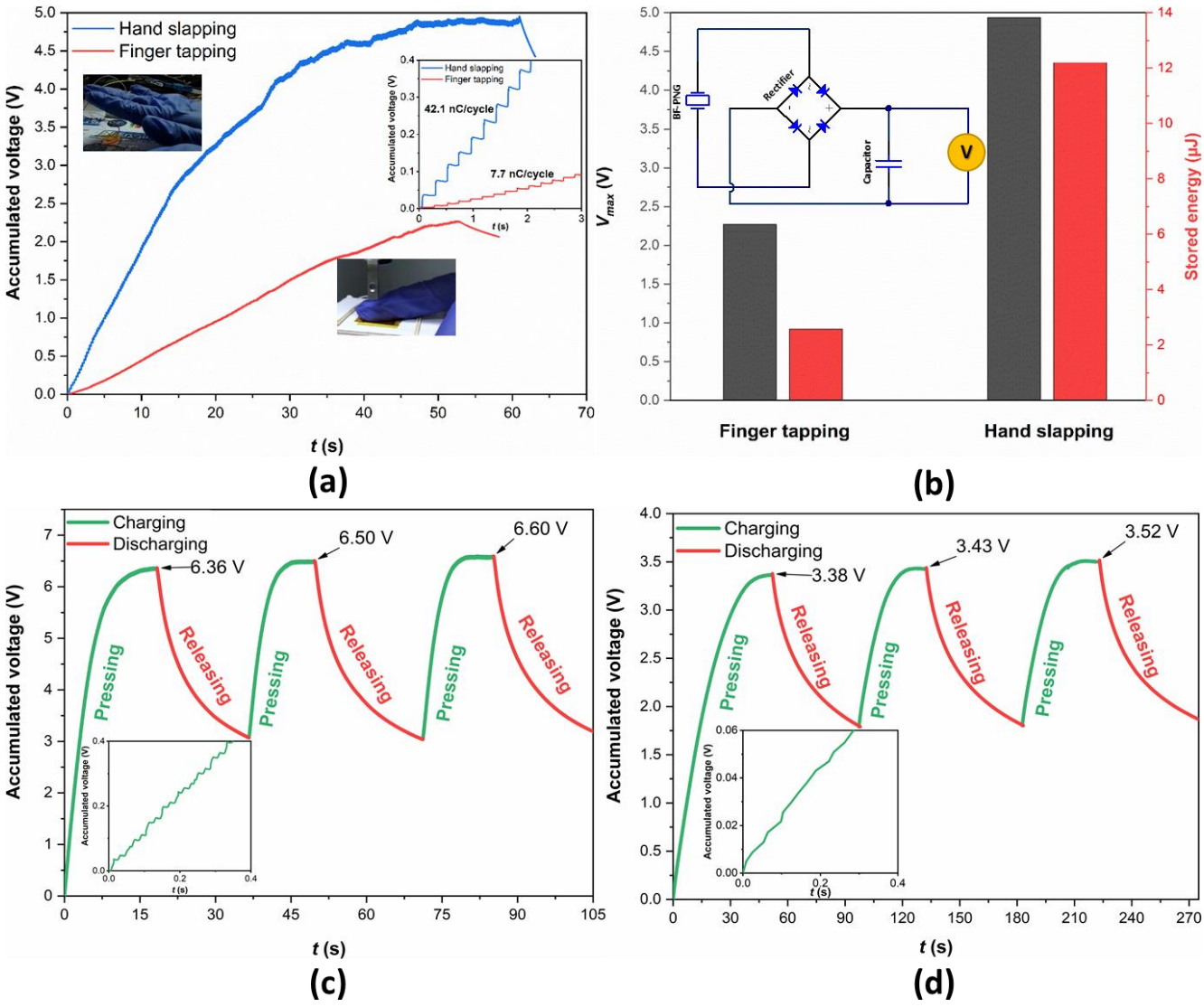

Fig. 6. (a) The accumulated voltage across a single capacitor of 1 μF charged by the BF-PNG at 4 Hz of imparting frequency under finger tapping and hand slapping, (b) the maximal output voltage and the equivalent stored energy (inset schematic circuit diagram of capacitor charging), and repeated charging and discharging shown for the (c) 1 μF and (d) 2.2 μF commercial capacitors charged by the BF-PNG at 23 Hz of sewing machine tapping frequency (insets show the zoomed portion of a charging curve).

3.4 Energy performances of BF-PNG

For a practical use of the harvested energy, the device cannot operate in open circuit, but instead must be connected to a load [57]. To examine the energy performances of BF-PNG, the output voltage characteristic was measured at various external resistive loads, as shown in the schematic circuit diagram in the inset of Fig. 7a. It is observed that the generated output voltage from the BF-PNG across a load resistor gradually increases with increasing resistance to reach a maximum then decreases (Fig. 7a). The variation of the power (*P*) related to the external resistance is also depicted in Fig. 7a. *P*

increases with the increasing resistance up to a maximum value and then decreases by further increasing the resistance. The maximal power $P_{max} = V^2/R_L$ of 25 μW was reached at the resistive load R_L = 3.5 MΩ. It occurs when the value of the resistive load is equal to the impedance of the BF-PNG piezoelectric capacitor. The obtained P_{max} is more than three-fold higher than that obtained, by Baek et al. [58] in a piezoelectric nanogenerator based on encapsulated BCZT nanoparticles and Ag nanowires in the PDMS matrix at the resistive load R_L = 100 MΩ. Moreover, such low R_L is also enabling the BF-PNG as a high output power source, compared to previously reported PNGs in Table 1. This value is quite similar to that reported by Karan et al. [59] The area power density P^s_{max} = 12.82 μW/cm^2 and volumetric power density P^v_{max} = 7.54 mW/cm^3 were estimated by using the Eqs. (1) and (2),

$$P^s_{max} = \frac{V^2}{R_L \times area}, \qquad (1)$$

$$P^v_{max} = \frac{V^2}{R_L \times volume}. \qquad (2)$$

Here, the active volume of 1.5 cm × 1.3 cm × 17 μm of the BF-PNG was used.

Table 1 compares the energy harvesting performance of BF-PNG with other PNGs reported in the literature. The V_{oc} and I_{sc} of our BF-PNG are higher than that reported in [49,60–68] and lower than stated in refs [10,52,59,69,70]. The obtained power density in the BF-PNG is much higher than that reported in refs [10,52,59,69,70]. This is mainly due to the thinner nanocomposite film that was used to design our BF-PNG. As stated before, the biodegradable PLA leads to natural piezoelectricity that makes the BF-PNG a self- poled device. This eliminates the need for high electric fields, in contrast to the majority of PVDF or PDMS-based PNGs, which request a high electric field, high temperature and prolonged time during the poling process [10,52,65–68].

Table 1. Comparison of the energy harvesting performances of BF-PNG with other PNGs reported in the literature.

Piezoelectric nanogenerator	Poling conditions	R_L (MΩ)	V_{oc} (V)	I_{sc} (μA)	P^v_{max} (μW/cm^3)	Ref.
20 vol% B_NP@PDA/PLA (BF-PNG)	No poling	3.5	14.4	0.55	7540	This work
BZT-BCT/PVDF	35 kV/cm, 10 h, 130 °C	-	20.61	2.0	3450	[52]
Cu-BZT-BCT/PVDF	35 kV/cm, 10 h, 130 °C	-	18.8	1.84	4120	[52]
BCZT nanofibers/PVDFHFP composite	20 kV/cm, 2 h, 50 °C	5.5	10	0.75	2.91	[68]
$BaTiO_3$ thin film	200 kV/cm, 15 h, 150 °C	-	1	0.026	7000	[60]
Oriented $BaTiO_3$ film	30 kV/cm, RT	80	6.5	0.14	105	[61]
BCZT nanowires	15 kV/cm, 2 h, 90 °C	-	3.25	0.055	338	[62]
ZnO nanowires	Not supplied	-	2.03	0.107	11000	[63]
PZT thin film	100 kV/cm, 3 h, 120 °C	200	200	1.5	1750	[69]
PZT/PVDF-HFP	250 kV/cm, 1 h, 150 °C	-	65.0	1.0	81.25	[10]
PZT/PET	40 kV/cm, 15 min, 130 °C	100	6.0	0.045	200	[64]
KNNS–BNKZ nanofibers	50 kV/cm, 150 °C, RT	100	10	-	4508	[49]
$KNbO_3$ nanowires/PDMS	50 kV/cm, 1 h, RT	10	10.5	1.3	42	[65]
$BaTiO_3$ nanotubes/PDMS	80 kV/cm, 12 h, RT	-	5.5	0.35	64	[66]
$KNbO_3$ nanorods/PDMS	150 kV/cm, 1 h, RT	-	3.2	0.0675	11.9	[67]
Chitin nanofiber/PDMS	Not supplied	-	22.0	0.12	97	[70]
Chitin nanofiber/PVDF/PDMS	Not supplied	-	49.0	1.9	6600	[70]
Eggshell membrane/PDMS	2 kV, 48 h	15	26.4	1.45	238.17	[59]

To support the analysis above and demonstrate the output performance of our BF-PNG to power commercial electronics, a visual and realistic application was devoted. The electrical energy produced from the finger tapping of the BF-PNG was successfully used to drive commercial red LED (light-emitting diode) connected to a 1 μF capacitor (Fig. 7b). This capacitor could be charged up to 2.8 V in 115 s under successive finger tapping at a frequency of 4 Hz, which corresponds to the stored energy of 3.92 μJ. The corresponding schematic circuit diagram and demonstration video for the LED lighting is included in Fig. S3 and Video 6 in the Supporting Information, respectively. Hence, the combination of BF-PNG and the energy storage device could cover a potential solution to the frequent replacement of the discharged batteries. Also, it can be of great potential for effective power generation and energy harvesting from human movements to power small portable electronics [71]. As reported by Hwang et al. [5] in the case of healthy animals, the minimum external electric energy needed to trigger the action potential required to contract the heart artificially is 1.1 μJ. Hence, the BF-PNG could be applicable for

biomedical sensors and actuators such as pacemakers. Moreover, the choice of biodegradable polymer (PLA) [32,72,73] that is extensively used in medicine and lead-free biocompatible ceramic (BCZT) [27–29] are encouraging for such applications.

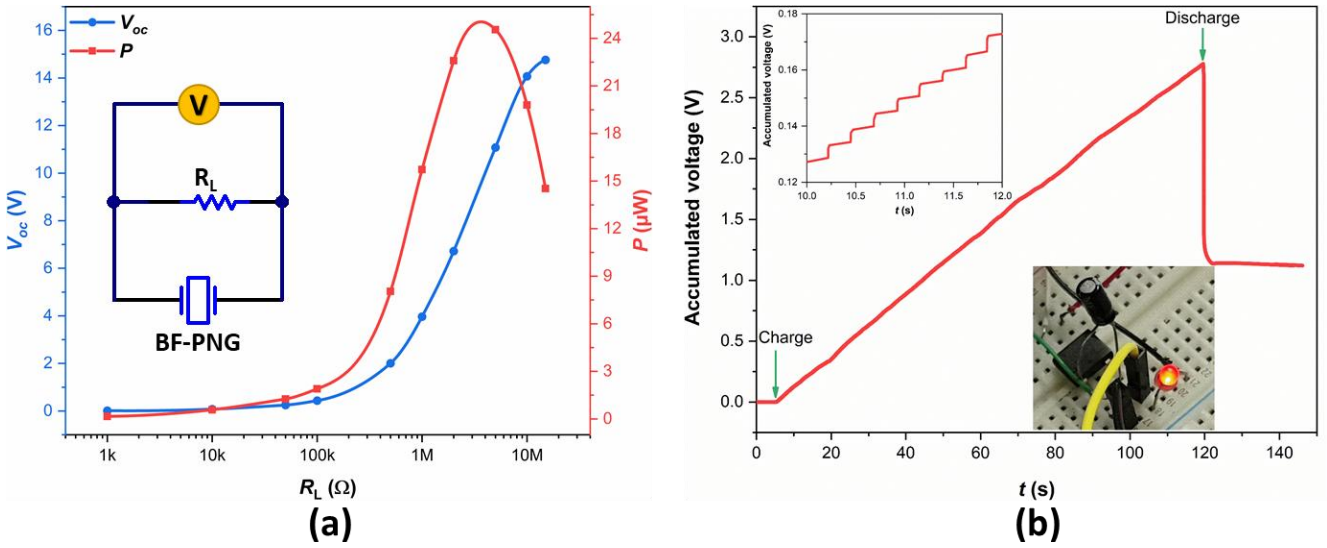

Fig. 7. (a) The output voltage and power density generated by the BF-PNG across various resistors (inset shows the schematic circuit diagram of the harvested output voltage), and (b) voltage charging curve of a 1 μF commercial capacitor by the BF-PNG under finger tapping at a frequency of 4 Hz. The upper inset shows an enlarged plot of voltage steps during capacitor charging. The lower inset depicts a digital photograph of a glowing red LED powered by the charged capacitor.

4. Conclusion

All-ecological piezoelectric nanogenerator was designed via core-shell structured BCZT filler with a PDA layer and a biodegradable PLA matrix. The piezoelectricity of BCZT@PDA nanoparticles before and after embedding in the PLA matrix was checked via measurements of the piezoelectric hysteresis loops by PFM. The designed BF-PNG could generate open-circuit voltage and short-circuit current of 14.4 V and 0.55 μA, respectively, under gentle finger tapping. Moreover, the BF-PNG demonstrated outstanding durability, high mechanical robustness, and stable output voltage even after 14000 cycles of high-frequency impartations. The maximum power density achieved was around 7.54 mW/cm^3 at a low resistive load of 3.5 MΩ. The feasibility of the BF-PNG was verified by trigging commercial electronics (charging capacitors and lighting an LED). The BF-PNG could drive a 1 μF capacitor to store the energy of 3.92 μJ within 115 s under gentle finger tapping. The reported nanocomposite film BF-PNG has the significant potential to be used as an energy source for self-powered medical devices.

Acknowledgements

The authors gratefully acknowledge the generous financial support of CNRST Priority Program PPR 15/2015, Slovenian Research Agency (programs P1-0125, P2-0105; ARRS young researcher project U.P), the European Union Horizon 2020 Research and Innovation actions MSCA-RISE-ENGIMA (No. 778072) and MSCA-RISE-MELON (No. 872631). H.U would like to thank Jena Cilenšek and Tjaša Klavžar for their technical assistance. Z.H would also like to thank Taha El Assimi for the contact force measurements.

References

[1] M.A. Parvez Mahmud, N. Huda, S.H. Farjana, M. Asadnia, C. Lang, Recent Advances in Nanogenerator-Driven Self-Powered Implantable Biomedical Devices, Adv. Energy Mater. 8 (2018) 1–25. doi:10.1002/aenm.201701210.

[2] D. Hu, M. Yao, Y. Fan, C. Ma, M. Fan, M. Liu, Strategies to achieve high performance piezoelectric nanogenerators, Nano Energy. 55 (2019) 288–304. doi:10.1016/j.nanoen.2018.10.053.

[3] Y. Zhang, M. Wu, Q. Zhu, F. Wang, H. Su, H. Li, C. Diao, H. Zheng, Y. Wu, Z.L. Wang, Performance Enhancement of Flexible Piezoelectric Nanogenerator via Doping and Rational 3D Structure Design For Self-Powered Mechanosensational System, Adv. Funct. Mater. 29 (2019) 1904259. doi:10.1002/adfm.201904259.

[4] Z. Zhou, Z. Zhang, Q. Zhang, H. Yang, Y. Zhu, Y. Wang, L. Chen, Controllable Core-Shell BaTiO3@Carbon Nanoparticle-Enabled P(VDF-TrFE) Composites: A Cost-Effective Approach to High-Performance Piezoelectric Nanogenerators, ACS Appl. Mater. Interfaces. 12 (2020) 1567–1576. doi:10.1021/acsami.9b18780.

[5] G.T. Hwang, H. Park, J.H. Lee, S. Oh, K. Il Park, M. Byun, H. Park, G. Ahn, C.K. Jeong, K. No, H. Kwon, S.G. Lee, B. Joung, K.J. Lee, Self-powered cardiac pacemaker enabled by flexible single crystalline PMN-PT piezoelectric energy harvester, Adv. Mater. 26 (2014) 4880–4887. doi:10.1002/adma.201400562.

[6] F.W. Horlbeck, F. Mellert, J. Kreuz, G. Nickenig, J.O. Schwab, Real-world data on the lifespan of implantable cardioverter-defibrillators depending on manufacturers and the amount of ventricular pacing, J. Cardiovasc. Electrophysiol. 23 (2012) 1336–1342. doi:10.1111/j.1540-8167.2012.02408.x.

[7] Z. Li, G. Zhu, R. Yang, A.C. Wang, Z.L. Wang, Muscle-driven in vivo nanogenerator, Adv. Mater. 22 (2010) 2534–2537. doi:10.1002/adma.200904355.

[8] D.H. Kim, H.J. Shin, H. Lee, C.K. Jeong, H. Park, G.T. Hwang, H.Y. Lee, D.J. Joe, J.H. Han, S.H. Lee, J. Kim, B. Joung, K.J. Lee, In Vivo Self-Powered Wireless Transmission Using Biocompatible Flexible Energy Harvesters, Adv. Funct. Mater. 27 (2017) 1700341. doi:10.1002/adfm.201700341.

[9] H. Feng, C. Zhao, P. Tan, R. Liu, X. Chen, Z. Li, Nanogenerator for Biomedical Applications, Adv. Healthc. Mater. 7 (2018) 1–18. doi:10.1002/adhm.201701298.

[10] X. Niu, W. Jia, S. Qian, J. Zhu, J. Zhang, X. Hou, J. Mu, W. Geng, J. Cho, J. He, X. Chou, High-Performance PZT-Based Stretchable Piezoelectric Nanogenerator, ACS Sustain. Chem. Eng. 7 (2019) 979–985. doi:10.1021/acssuschemeng.8b04627.

[11] Y. Liu, L. Zhao, L. Wang, H. Zheng, D. Li, R. Avila, K.W.C. Lai, Z. Wang, Z. Xie, Y. Zi, X. Yu, Skin-Integrated Graphene-Embedded Lead Zirconate Titanate Rubber for Energy Harvesting and Mechanical Sensing, Adv. Mater. Technol. 4 (2019) 1900744. doi:10.1002/admt.201900744.

[12] Binoy Bera, Recent Advances In Piezoelectric Nano generators In Energy Harvesting Applications BinoyBera, Imp. J. Interdiscip. Res. . 2 (2016) 1274–1291.

[13] Z. Hanani, D. Mezzane, M. Amjoud, S. Fourcade, A.G. Razumnaya, I.A. Luk'yanchuk, M. Gouné, Enhancement of dielectric properties of lead-free BCZT ferroelectric ceramics by grain size engineering, Superlattices Microstruct. 127 (2019) 109–117. doi:10.1016/j.spmi.2018.03.004.

[14] J. Wu, Historical Introduction, in: Adv. Lead-Free Piezoelectric Mater., Springer Singapore, Singapore, 2018: pp. 1–40. doi:10.1007/978-981-10-8998-5_1.

[15] Z. Hanani, D. Mezzane, M. Amjoud, A.G.G. Razumnaya, S. Fourcade, Y. Gagou, K. Hoummada, M. El Marssi, M. Gouné, Phase transitions, energy storage performances and electrocaloric effect of the lead-free Ba0.85Ca0.15Zr0.10Ti0.90O3 ceramic relaxor, J. Mater. Sci. Mater. Electron. 30 (2019) 6430–6438. doi:10.1007/s10854-019-00946-5.

[16] L.-Q. Cheng, J.-F. Li, A review on one dimensional perovskite nanocrystals for piezoelectric applications, J. Mater. 2 (2016) 25–36. doi:10.1016/j.jmat.2016.02.003.

[17] S. Siddiqui, D. Il Kim, E. Roh, L.T. Duy, T.Q. Trung, M.T. Nguyen, N.E. Lee, A durable and stable piezoelectric nanogenerator with nanocomposite nanofibers embedded in an elastomer under high loading for a self-powered sensor system, Nano Energy. 30 (2016) 434–442. doi:10.1016/j.nanoen.2016.10.034.

[18] P.K. Panda, B. Sahoo, PZT to lead free piezo ceramics: A review, Ferroelectrics. 474 (2015) 128–143. doi:10.1080/00150193.2015.997146.

[19] X. Ji, C. Wang, S. Zhang, R. Tu, Q. Shen, J. Shi, L. Zhang, Structural and electrical properties of BCZT ceramics synthesized by sol–gel-hydrothermal process at low temperature, J. Mater. Sci. Mater. Electron. 30 (2019) 12197–12203. doi:10.1007/s10854-019-01578-5.

[20] Z. Hanani, S. Merselmiz, A. Danine, N. Stein, D. Mezzane, M. Amjoud, M. Lahcini, Y. Gagou, M. Spreitzer, D. Vengust, Z. Kutnjak, M. El Marssi, I.A. Luk'yanchuk, M. Gouné, Enhanced dielectric and electrocaloric properties in lead-free rod-like BCZT ceramics, J. Adv. Ceram. 9 (2020) 210–219. doi:10.1007/s40145-020-0361-1.

[21] W. Cai, Q. Zhang, C. Zhou, R. Gao, S. Zhang, Z. Li, R. Xu, G. Chen, X. Deng, Z. Wang, C. Fu, Synergistic effect of grain size and phase boundary on energy storage performance and electric properties of BCZT ceramics, J. Mater. Sci. Mater. Electron. 31 (2020) 9167–9175. doi:10.1007/s10854-020-03446-z.

[22] W. Liu, X. Ren, Large piezoelectric effect in Pb-free ceramics, Phys. Rev. Lett. 103 (2009) 257602. doi:10.1103/PhysRevLett.103.257602.

[23] M. ben Abdessalem, I. Kriaa, A. Aydi, N. Abdelmoula, Large electrocaloric effect in lead-free Ba1-xCaxTi1-yZryO3 ceramics under strong electric field at room-temperature, Ceram. Int. 44 (2018) 13595–13601. doi:10.1016/j.ceramint.2018.04.194.

[24] S. Patel, D. Sharma, A. Singh, R. Vaish, Enhanced thermal energy conversion and dynamic hysteresis behavior of Sr-added Ba0.85Ca0.15Ti0.9Zr0.1O3 ferroelectric ceramics, J. Mater. 2 (2016) 75–86. doi:10.1016/j.jmat.2016.01.002.

[25] J.P. Praveen, T. Karthik, A.R. James, E. Chandrakala, S. Asthana, D. Das, Effect of poling process on piezoelectric properties of sol-gel derived BZT-BCT ceramics, J. Eur. Ceram. Soc. 35 (2015) 1785–1798. doi:10.1016/j.jeurceramsoc.2014.12.010.

[26] F. Wang, W. Li, H. Jiang, M. Xue, J. Lu, J. Yao, Preparation and dielectric properties of

Ba0.95Ca0.05Ti0.8Zr0.2O3-polyethersulfone composites, J. Appl. Phys. 107 (2010) 043528. doi:10.1063/1.3280017.

[27] K.K. Poon, M.C. Wurm, D.M. Evans, M.A. Einarsrud, R. Lutz, J. Glaum, Biocompatibility of (Ba,Ca)(Zr,Ti)O3 piezoelectric ceramics for bone replacement materials, J. Biomed. Mater. Res. - Part B Appl. Biomater. 108 (2019) 1295–1303. doi:10.1002/jbm.b.34477.

[28] C.S. Manohar, B.S. Kumar, S.P.P. Sadhu, S.K. Srimadh, V.S. Muthukumar, S. Venketesh, K.B.R. Varma, Novel Lead-free biocompatible piezoelectric Hydroxyapatite (HA)-BCZT (Ba0.85Ca0.15Zr0.1Ti0.9O3) nanocrystal composites for bone regeneration, Nanotechnol. Rev. 8 (2019) 61–78. doi:10.1515/ntrev-2019-0006.

[29] N.D. Scarisoreanu, F. Craciun, V. Ion, R. Birjega, A. Bercea, V. Dinca, M. Dinescu, L.E. Sima, M. Icriverzi, A. Roseanu, L. Gruionu, G. Gruionu, Lead-Free Piezoelectric (Ba,Ca)(Zr,Ti)O3 Thin Films for Biocompatible and Flexible Devices, ACS Appl. Mater. Interfaces. 9 (2017) 266–278. doi:10.1021/acsami.6b14774.

[30] I. Navarro-Baena, V. Sessini, F. Dominici, L. Torre, J.M. Kenny, L. Peponi, Design of biodegradable blends based on PLA and PCL: From morphological, thermal and mechanical studies to shape memory behavior, Polym. Degrad. Stab. 132 (2016) 97–108. doi:10.1016/j.polymdegradstab.2016.03.037.

[31] S. Saravanamoorthy, M. Muneeswaran, N.V. Giridharan, S. Velmathi, Solvent-free ring opening polymerization of ε-caprolactone and electrical properties of polycaprolactone blended BiFeO3 nanocomposites, RSC Adv. 5 (2015) 43897–43905. doi:10.1039/c5ra03983e.

[32] H. Zhou, J.G. Lawrence, S.B. Bhaduri, Fabrication aspects of PLA-CaP/PLGA-CaP composites for orthopedic applications: A review, Acta Biomater. 8 (2012) 1999–2016. doi:10.1016/j.actbio.2012.01.031.

[33] K. Shinyama, S. Fujita, Study on the electrical properties of a biodegradable plastic, in: Proc. IEEE Int. Conf. Prop. Appl. Dielectr. Mater., 2003: pp. 707–710. doi:10.1109/icpadm.2003.1218515.

[34] S.M. Lebedev, O.S. Gefle, E.T. Amitov, D.Y. Berchuk, D. V. Zhuravlev, Poly(lactic acid)-based polymer composites with high electric and thermal conductivity and their characterization, Polym. Test. 58 (2017) 241–248. doi:10.1016/j.polymertesting.2016.12.033.

[35] S. Mishra, L. Unnikrishnan, S.K. Nayak, S. Mohanty, Advances in Piezoelectric Polymer Composites for Energy Harvesting Applications: A Systematic Review, Macromol. Mater. Eng. 304 (2019) 1800463. doi:10.1002/mame.201800463.

[36] S. Gong, B. Zhang, J. Zhang, Z.L. Wang, K. Ren, Biocompatible Poly(lactic acid)-Based Hybrid Piezoelectric and Electret Nanogenerator for Electronic Skin Applications, Adv. Funct. Mater. 30 (2020) 1908724. doi:10.1002/adfm.201908724.

[37] X. Li, S. Chen, X. Zhang, J. Li, H. Liu, N. Han, X. Zhang, Poly-l-Lactic Acid/Graphene Electrospun Composite Nanofibers for Wearable Sensors, Energy Technol. 8 (2020) 1901252. doi:10.1002/ente.201901252.

[38] M. Ando, S. Takeshima, Y. Ishiura, K. Ando, O. Onishi, Piezoelectric antibacterial fabric comprised of poly(L-lactic acid) yarn, Jpn. J. Appl. Phys. 56 (2017) 10PG01. doi:10.7567/JJAP.56.10PG01.

[39] E.J. Curry, K. Ke, M.T. Chorsi, K.S. Wrobel, A.N. Miller, A. Patel, I. Kim, J. Feng, L. Yue, Q. Wu, C.L. Kuo, K.W.H. Lo, C.T. Laurencin, H. Ilies, P.K. Purohit, T.D. Nguyen, Biodegradable piezoelectric force sensor, Proc. Natl. Acad. Sci. U. S. A. 115 (2018) 909–914. doi:10.1073/pnas.1710874115.

[40] Q. Zheng, Y. Zou, Y. Zhang, Z. Liu, B. Shi, X. Wang, Y. Jin, H. Ouyang, Z. Li, Z.L. Wang, Biodegradable triboelectric nanogenerator as a life-time designed implantable power source, Sci. Adv. 2 (2016) 1–10. doi:10.1126/sciadv.1501478.

[41] Z. Hanani, D. Mezzane, M. Amjoud, Y. Gagou, K. Hoummada, C. Perrin, A.G. Razumnaya, Z. Kutnjak, A. Bouzina, M. El Marssi, M. Gouné, B. Rožič, Structural, dielectric, and ferroelectric properties of lead-free BCZT ceramics elaborated by low-temperature hydrothermal processing, J. Mater. Sci. Mater. Electron. 31 (2020) 10096–10104. doi:10.1007/s10854-020-03555-9.

[42] Z. Hanani, S. Merselmiz, D. Mezzane, M. Amjoud, A. Bradeško, B. Rožič, M. Lahcini, M. El Marssi, A. V. Ragulya, I.A. Luk'yanchuk, Z. Kutnjak, M. Gouné, Thermally-stable high energy storage performances and large electrocaloric effect over a broad temperature span in lead-free BCZT ceramic, RSC Adv. 10 (2020) 30746–30755. doi:10.1039/D0RA06116F.

[43] Z. Hanani, E.H. Ablouh, M. 'barek Amjoud, D. Mezzane, S. Fourcade, M. Gouné, Very-low temperature synthesis of pure and crystalline lead-free Ba.85Ca.15Zr.1Ti.9O3 ceramic, Ceram. Int. 44 (2018) 10997–11000. doi:10.1016/j.ceramint.2018.03.022.

[44] M.M. Kržmanc, B. Jančar, H. Uršič, M. Tramšek, D. Suvorov, Tailoring the Shape, Size, Crystal Structure, and Preferential Growth Orientation of BaTiO3 Plates Synthesized through a Topochemical Conversion Process, Cryst. Growth Des. 17 (2017) 3210–3220. doi:10.1021/acs.cgd.7b00164.

[45] M.M. Kržmanc, H. Uršič, A. Meden, R.C. Korošec, D. Suvorov, Ba1-xSrxTiO3 plates: Synthesis through topochemical conversion, piezoelectric and ferroelectric characteristics, Ceram. Int. 44 (2018) 21406–21414. doi:10.1016/j.ceramint.2018.08.198.

[46] X. Ni, F. Wang, A. Lin, Q. Xu, Z. Yang, Y. Qin, Flexible nanogenerator based on single BaTiO3 nanowire, Sci. Adv. Mater. 5 (2013) 1781–1787. doi:10.1166/sam.2013.1629.

[47] F. Wang, Y.W. Mai, D. Wang, R. Ding, W. Shi, High quality barium titanate nanofibers for flexible piezoelectric device applications, Sensors Actuators, A Phys. 233 (2015) 195–201. doi:10.1016/j.sna.2015.07.002.

[48] C. Hu, L. Cheng, Z. Wang, Y. Zheng, S. Bai, Y. Qin, A Transparent Antipeep Piezoelectric Nanogenerator to Harvest Tapping Energy on Screen, Small. 12 (2016) 1315–1321. doi:10.1002/smll.201502453.

[49] R. Zhu, J. Jiang, Z. Wang, Z. Cheng, H. Kimura, High output power density nanogenerator based on lead-free 0.96(K0.48Na0.52)(Nb0.95Sb0.05)O3-0.04Bi0.5(Na0.82K0.18)0.5ZrO3 piezoelectric nanofibers, RSC Adv. 6 (2016) 66451–66456. doi:10.1039/c6ra12123c.

[50] F. Bernard, L. Gimeno, B. Viala, B. Gusarov, O. Cugat, Direct Piezoelectric Coefficient Measurements of PVDF and PLLA under Controlled Strain and Stress, Proceedings. 1 (2017) 335. doi:10.3390/proceedings1040335.

[51] C. Zhao, J. Zhang, Z.L. Wang, K. Ren, A Poly(l -Lactic Acid) Polymer-Based Thermally Stable Cantilever for Vibration Energy Harvesting Applications , Adv. Sustain. Syst. 1 (2017) 1700068. doi:10.1002/adsu.201700068.

[52] D.J. Shin, J.H. Ji, J. Kim, G.H. Jo, S.J. Jeong, J.H. Koh, Enhanced flexible piezoelectric energy harvesters based on BaZrTiO3–BaCaTiO3 nanoparticles/PVDF composite films with Cu floating electrodes, J. Alloys Compd. 802 (2019) 562–572. doi:10.1016/j.jallcom.2019.05.363.

[53] L. Gu, J. Liu, N. Cui, Q. Xu, T. Du, L. Zhang, Z. Wang, C. Long, Y. Qin, Enhancing the current density of a piezoelectric nanogenerator using a three-dimensional intercalation electrode, Nat.

Commun. 11 (2020) 1030. doi:10.1038/s41467-020-14846-4.

[54] S. Wang, L. Lin, Y. Xie, Q. Jing, S. Niu, Z.L. Wang, Sliding-triboelectric nanogenerators based on in-plane charge-separation mechanism, Nano Lett. 13 (2013) 2226–2233. doi:10.1021/nl400738p.

[55] S. Niu, Y.S. Zhou, S. Wang, Y. Liu, L. Lin, Y. Bando, Z.L. Wang, Simulation method for optimizing the performance of an integrated triboelectric nanogenerator energy harvesting system, Nano Energy. 8 (2014) 150–156. doi:10.1016/j.nanoen.2014.05.018.

[56] S. Niu, S. Wang, L. Lin, Y. Liu, Y.S. Zhou, Y. Hu, Z.L. Wang, Theoretical study of contact-mode triboelectric nanogenerators as an effective power source, Energy Environ. Sci. 6 (2013) 3576–3583. doi:10.1039/c3ee42571a.

[57] J. Briscoe, N. Jalali, P. Woolliams, M. Stewart, P.M. Weaver, M. Cain, S. Dunn, Measurement techniques for piezoelectric nanogenerators, Energy Environ. Sci. 6 (2013) 3035–3045. doi:10.1039/c3ee41889h.

[58] C. Baek, J.H. Yun, J.E. Wang, C.K. Jeong, K.J. Lee, K. Il Park, D.K. Kim, A flexible energy harvester based on a lead-free and piezoelectric BCTZ nanoparticle-polymer composite, Nanoscale. 8 (2016) 17632–17638. doi:10.1039/c6nr05784e.

[59] S.K. Karan, S. Maiti, S. Paria, A. Maitra, S.K. Si, J.K. Kim, B.B. Khatua, A new insight towards eggshell membrane as high energy conversion efficient bio-piezoelectric energy harvester, Mater. Today Energy. 9 (2018) 114–125. doi:10.1016/j.mtener.2018.05.006.

[60] K. Il Park, S. Xu, Y. Liu, G.T. Hwang, S.J.L. Kang, Z.L. Wang, K.J. Lee, Piezoelectric BaTiO3 thin film nanogenerator on plastic substrates, Nano Lett. 10 (2010) 4939–4943. doi:10.1021/nl102959k.

[61] T. Gao, J. Liao, J. Wang, Y. Qiu, Q. Yang, M. Zhang, Y. Zhao, L. Qin, H. Xue, Z. Xiong, L. Chen, Q.M. Wang, Highly oriented BaTiO3 film self-assembled using an interfacial strategy and its application as a flexible piezoelectric generator for wind energy harvesting, J. Mater. Chem. A. 3 (2015) 9965–9971. doi:10.1039/c5ta01079a.

[62] W. Wu, L. Cheng, S. Bai, W. Dou, Q. Xu, Z. Wei, Y. Qin, Electrospinning lead-free 0.5Ba(Zr0.2Ti0.8)O3-0.5(Ba0.7Ca0.3)TiO3 nanowires and their application in energy harvesting, J. Mater. Chem. A. 1 (2013) 7332–7338. doi:10.1039/c3ta10792b.

[63] G. Zhu, R. Yang, S. Wang, Z.L. Wang, Flexible high-output nanogenerator based on lateral ZnO nanowire array, Nano Lett. 10 (2010) 3151–3155. doi:10.1021/nl101973h.

[64] W. Wu, S. Bai, M. Yuan, Y. Qin, Z.L. Wang, T. Jing, Lead zirconate titanate nanowire textile nanogenerator for wearable energy-harvesting and self-powered devices, ACS Nano. 6 (2012) 6231–6235. doi:10.1021/nn3016585.

[65] M.R. Joung, H. Xu, I.T. Seo, D.H. Kim, J. Hur, S. Nahm, C.Y. Kang, S.J. Yoon, H.M. Park, Piezoelectric nanogenerators synthesized using KNbO3 nanowires with various crystal structures, J. Mater. Chem. A. 2 (2014) 18547–18553. doi:10.1039/c4ta03551h.

[66] Z.H. Lin, Y. Yang, J.M. Wu, Y. Liu, F. Zhang, Z.L. Wang, BaTiO3 nanotubes-based flexible and transparent nanogenerators, J. Phys. Chem. Lett. 3 (2012) 3599–3604. doi:10.1021/jz301805f.

[67] J.H. Jung, C.Y. Chen, B.K. Yun, N. Lee, Y. Zhou, W. Jo, L.J. Chou, Z.L. Wang, Lead-free KNbO3 ferroelectric nanorod based flexible nanogenerators and capacitors, Nanotechnology. 23 (2012) 375401. doi:10.1088/0957-4484/23/37/375401.

[68] K.S. Chary, V. Kumar, C.D. Prasad, H.S. Panda, Dopamine-modified Ba0.85Ca0.15Zr0.1Ti0.9O3 ultra-fine fibers/PVDF-HFP composite–based nanogenerator: synergistic effect on output electric signal, J. Aust. Ceram. Soc. (2020). doi:10.1007/s41779-020-00458-0.

[69] K. Il Park, J.H. Son, G.T. Hwang, C.K. Jeong, J. Ryu, M. Koo, I. Choi, S.H. Lee, M. Byun, Z.L. Wang, K.J. Lee, Highly-efficient, flexible piezoelectric PZT thin film nanogenerator on plastic substrates, Adv. Mater. 26 (2014) 2514–2520. doi:10.1002/adma.201305659.

[70] N.A. Hoque, P. Thakur, P. Biswas, M.M. Saikh, S. Roy, B. Bagchi, S. Das, P.P. Ray, Biowaste crab shell-extracted chitin nanofiber-based superior piezoelectric nanogenerator, J. Mater. Chem. A. 6 (2018) 13848–13858. doi:10.1039/c8ta04074e.

[71] S.K. Si, S.K. Karan, S. Paria, A. Maitra, A.K. Das, R. Bera, A. Bera, L. Halder, B.B. Khatua, A strategy to develop an efficient piezoelectric nanogenerator through ZTO assisted γ-phase nucleation of PVDF in ZTO/PVDF nanocomposite for harvesting bio-mechanical energy and energy storage application, Mater. Chem. Phys. 213 (2018) 525–537. doi:10.1016/j.matchemphys.2018.04.013.

[72] A.J.R. Lasprilla, G.A.R. Martinez, B.H. Lunelli, A.L. Jardini, R.M. Filho, Poly-lactic acid synthesis for application in biomedical devices - A review, Biotechnol. Adv. 30 (2012) 321–328. doi:10.1016/j.biotechadv.2011.06.019.

[73] P. Saini, M. Arora, M.N.V.R. Kumar, Poly(lactic acid) blends in biomedical applications, Adv. Drug Deliv. Rev. 107 (2016) 47–59. doi:10.1016/j.addr.2016.06.014.